THIS MONTH IN

JNM

In vivo tracking of cellular therapy: Aarntzen and colleagues review recent innovations in transplantation of living cells that advance regeneration of damaged tissue, replace function, and redirect aberrant processes . . . ***Page 1825***

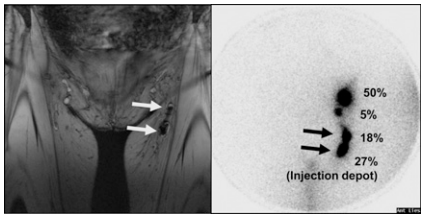

PET/CT and MTV in myeloma: Fonti and colleagues report on whether metabolic tumor volume as determined by ^{18}F-FDG PET/CT can be used to predict progression-free and overall survival in patients with multiple myeloma . . . . . ***Page 1829***

PET and MEK inhibition: Kraeber-Bodéré and colleagues use ^{18}F-FDG PET to assess 2 mitogen-activated protein kinase kinase inhibitors in separate trials to show the potential of metabolic imaging for dose considerations, compound selection, and response prediction in early trials. . . . . ***Page 1836***

PET/CT meta-analysis: Xu and colleagues offer a systematic review and analysis of the performance of whole-body PET/CT for detection of distant malignancies in various cancers . . . . . ***Page 1847***

Thyroid uptake in breast cancer: Kim and colleagues explore the prognostic value of incidental diffuse thyroid ^{18}F-FDG uptake related to autoimmune thyroiditis in PET imaging in patients with breast cancer . . . . . ***Page 1855***

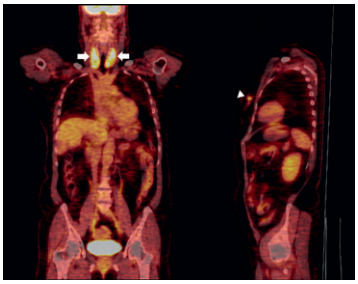

^{18}F-FDG and ^{18}F-DOPA PET in MTC: Verbeek and colleagues compare these 2 PET tracers with biochemical parameters and survival in patients with medullary thyroid carcinoma to assess potential utility in detecting progressive disease . . . . . ***Page 1863***

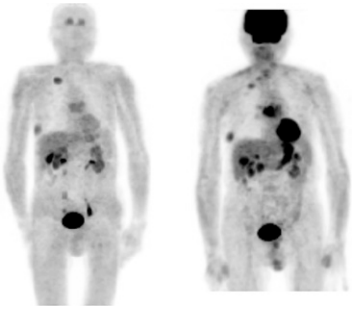

Integrin imaging in DTC: Zhao and colleagues evaluate integrin $\alpha_v\beta_3$ imaging in the detection of radioactive iodine–refractory differentiated thyroid cancer lesions and resultant identification of feasible antiangiogenic therapeutic targets. . . . . ***Page 1872***

Segmentation-based AC in PET/MRI: Kim and colleagues analyze potential bias in standardized uptake value estimation using 4 different segmentation-based attenuation correction methods on data from cancer patients with bone and liver lesions. . . . . ***Page 1878***

^{18}F-DCFBC tumor detection and dosimetry: Cho and colleagues describe initial clinical experiences with and radiation dosimetry of this PET tracer, a low-molecular-weight, urea-based inhibitor of prostate-specific membrane antigen, in men with prostate cancer . . . . . ***Page 1883***

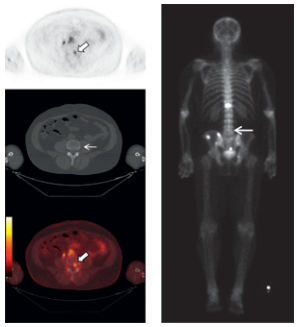

Gating error and cardiac dyssynchrony: Ludwig and colleagues examine the incidence and effect of gating errors on SPECT quantification of left ventricular mechanical dyssynchrony and test a possible solution for affected studies . . . . . ***Page 1892***

Performance of high-sensitivity cameras: Imbert and colleagues analyze both phantom and human images to compare the performance of 3 cadmium-zinc-telluride cameras/collimation systems recently commercialized for myocardial SPECT . . . . . ***Page 1897***

^{18}F-FLT PET and survival in glioma: Idema and colleagues assess various ^{18}F-FLT PET segmentation methods to estimate proliferative volume and its prognostic value for overall survival in patients with suspected high-grade glioma. . . . . ***Page 1904***

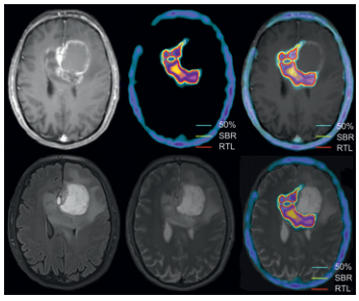

^{18}F-FLT PET in glioma: Yamamoto and colleagues evaluate ^{18}F-FLT uptake on PET in patients with newly diagnosed and recurrent gliomas and correlate the results with tumor grade and proliferative activity . . . . . ***Page 1911***

PET/MRI for neurologic applications: Catana and colleagues provide an educational overview of methodologic improvements in hybrid PET/MRI and discuss potential neurologic and psychiatric applications. . . . . ***Page 1916***

Pretargeted immuno-SPECT: Schoffelen and colleagues describe the use of pretargeted immuno-SPECT with TF2 and ^{111}In- or ^{177}Lu-IMP288 to predict and confirm tumor targeting and monitor the therapeutic effect of radioimmunotherapy . . . . . ***Page 1926***

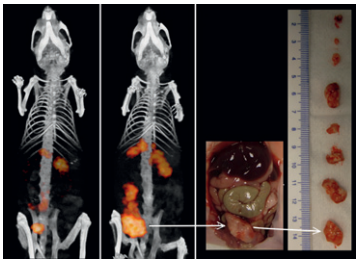

Imaging radiovirotherapy: Haddad and colleagues assess the feasibility and parameters of serial imaging and long-term monitoring of virotherapy and response of pancreatic cancer xenografts treated with a vaccinia virus carrying the human sodium iodide symporter GLV-1h153. . . . . ***Page 1933***

HER2–HER3 bispecific radioimmunoconjugates: Razumienko and colleagues construct agents and use SPECT/CT to evaluate tumor imaging in athymic mice that express one or both human epidermal growth factor receptors . . . . . ***Page 1943***

Matched terbium radionuclide quadruplet: Müller and colleagues describe a proof-of-concept study designed to produce 4 terbium radioisotopes and assess their diagnostic and therapeutic features in vivo when labeled with a folate-based targeting agent . . . . . ***Page 1951***

GLP-1R PET in myocardial ischemia: Gao and colleagues use noninvasive PET to monitor the presence and time course of regional myocardial glucagonlike peptide 1 receptor expression after myocardial ischemia or reperfusion . . . . . ***Page 1960***

^{123}I-5I-R91150 SPECT after morphine: Adriaens and colleagues use SPECT and a radiolabeled 5-HT_{2A} radioligand to assess the influence of systemic morphine on cerebral 5-hydroxytryptamine receptor 2A binding in dogs. . . . . ***Page 1969***

$GABA_A$ receptor density in epilepsy: Syvänen and colleagues investigate whether flumazenil blood–brain barrier transport and binding to the benzodiazepine site on the γ-aminobutyric acid A receptor complex is altered in epilepsy and explore implications for ^{11}C-flumazenil PET interpretation. . . . . ***Page 1974***

Hyperoxic lung injury imaging: Clough and colleagues describe changes in lung uptake of ^{99m}Tc-HMPAO and ^{99m}Tc-duramycin, a new marker of cell injury, in rats exposed to hyperoxia for prolonged periods . . . . . ***Page 1984***

ON THE COVER

In this PET/MRI study of an epilepsy patient, a distinctly hypometabolic area typically corresponding to an epileptogenic focus is seen in the left temporal lobe.

See page 1923.